Dual-Purpose Nonoverlapping Coil Sets as Metal Object and Vehicle Position Detections for Wireless Stationary EV Chargers

Seog Y. Jeong, *Student Member, IEEE*, Hyung G. Kwak, *Student Member, IEEE*, Gi C. Jang, *Student Member, IEEE*, Su Y. Choi, *Member, IEEE*, and Chun T. Rim, *Senior Member, IEEE*

***Abstract*—For commercialization of wireless stationary electric vehicles (EV) chargers, metal object detection (MOD) on a power supply coil and detection of position (DoP) of EVs are needed. In this paper, dual-purpose nonoverlapping coil sets for both MOD and DoP, which detect a variation of magnetic flux on the power supply coil, are newly proposed, where the proposed MOD and DoP methods make no contribution to any power losses. The existence of metal objects on the power supply coil is determined by an induced voltage difference of the nonoverlapping coil sets, whereas the position of the EV is determined by an induced voltage of the nonoverlapping coil sets. A sensing circuit, which has a variable resistor that is different from the conventional overlapping coil for MOD, can make the induced voltage difference zero even when the magnetic flux distribution is distorted by moving the pick-up coil. The proposed nonoverlapping coil sets with the sensing circuit have been demonstrated by simulations and experiments. When metallic coins and aluminum sheets are located on the power supply coil, the induced voltage difference of the coil sets, which is ideally zero without metal objects, significantly increases to 62.8 and 450 mV, respectively, which is more than ten times the value without metal objects throughout experiments. In addition, when the pick-up coil approaches the power supply coil, induced voltage of each coil set increased roughly 1.6 times at 10 cm air gap.**

***Index Terms*—Detection of position (DoP), foreign object detection (FOD), inductive power transfer (IPT), metal object detection (MOD).**

Manuscript received June 19, 2017; revised September 1, 2017; accepted October 18, 2017. Date of publication October 22, 2017; date of current version June 22, 2018. The paper is original, but part of it has been presented at the 2015 IEEE WoW [12]. This work was supported by the Technology Innovation Program funded by the Ministry of Trade, Industry & Energy (South Korea) under Grant 20161210200740. Recommended for publication by Associate Editor S. K. Panda. *(Corresponding author: Seog Y. Jeong.)*

S. Y. Jeong and H. G. Kwak are with the Department of Nuclear and Quantum Engineering, Korea Advanced Institute of Science and Technology, Daejeon 305-755, South Korea (e-mail: seogyong@kaist.ac.kr; khk0787@kaist.ac.kr).

G. C. Jang is with Hyundai KEFICO, Gunpo 15859, South Korea (e-mail: GiChan.Jang@kefico.co.kr).

S. Y. Choi is with the Hyper Tube eXpress Research Team, Korea Railroad Research Institute, Uiwang 16105, South Korea (e-mail: suchoi@krri.re.kr).

C. T. Rim is with the Graduate Program of Energy Technology, Gwangju Institute of Science and Technology, Gwangju 305-755, South Korea (e-mail: ctrim@gist.ac.kr).

Color versions of one or more of the figures in this paper are available online at http://ieeexplore.ieee.org.

Digital Object Identifier 10.1109/TPEL.2017.2765521

I. Introduction

As GLOBAL warming and air pollution are becoming significant issues, transportation based on internal combustion engines is being recognized as a major contributor to these problems. In order to replace internal combustion vehicles, electric vehicles (EVs) such as pure EVs (PEVs), hybrid EVs (HEVs), and plug-in HEVs (PHEVs) have been developed. Among them, PHEVs are considered the most practical alternative for the near future transportation market because of their high energy efficiency and relatively low dependence on a battery compared to PEVs [1]–[4]. Conductive EV chargers based on ac or dc connectors have been commercialized, but they are not widely used by the public due to their heavy and inconvenient charging cables [5], [6]. As a solution for this problem, wireless stationary EV chargers using an inductive power transfer system (IPTS), which generally includes a power supply coil and a pick-up coil, have been developed [7], [8].

For commercialization of wireless stationary EV chargers, foreign object detection (FOD), which involves detecting metallic and living objects, is one of the practical issues. To prevent metallic object combustion due to eddy current losses during EV charging, several metal object detection (MOD) methods have been introduced to solve the combustion problem [9]–[12]. A basic MOD method is to compare power losses with and without metal objects. Due to its simple operation and cost-effectiveness, it has already been applied to the Qi standard for FOD [9]. However, this method is not suitable for high power applications such as wireless stationary EV chargers, because the portion of power loss of metal objects is too small, compared to the total power transfer capability. Another group of MOD methods is based on measuring the voltage, current, power, phase, and frequency of the resonators or quality factor for the pick-up coil with and without metal objects. However, these methods have only been validated for fixed wireless power transfer applications since the parameters including the quality factor of IPTS are changed by the position of the pick-up coil as well as the state of charge of the battery.

WiTricity, meanwhile, has developed an MOD system that has an overlapping coil structure comprising two reverse direction loops based on the variation of the magnetic flux on the power supply coil [11]. By magnetic field cancellation, the induced voltage of the overlapping coil will be zero for a

uniform magnetic flux distribution in the absence of metal objects. Magnetic fluxes are disturbed by the eddy current of a metal object when a metal object is situated on the overlapping coil, resulting in variation of the induced voltage. It is suitable for high power IPTS because there is contribution to power losses and no hindrance to power transfer. However, it still suffers from an imbalanced induced voltage problem due to the asymmetrical distribution of magnetic flux on the power supply coil, which results in malfunction of MOD. A detailed description of this critical problem will be presented in the next section. Moreover, the overlapping sensing coil wastes at least two layers of a printed circuit board (PCB) without any additional role. In addition to MOD, detection of position (DoP) of an EV to align the power supply coil and the pick-up coil for efficient power transfer is also important for commercialization of wireless stationary EV chargers. Many techniques for judging the existence of EVs have been studied to control each segmented power system for dynamic charging [13]–[25]. For wireless stationary charging systems, where it is important to find the exact position of EVs, adoption of expensive equipment such as video cameras, RFIDs, and optical sensors is considered [14]–[17]. Along with their high cost, complexity of operations, and difficulties in integrating with the power supply coil, however, the option is not well accepted because of malfunction that often occurs due to dust or metal objects.

In this paper, novel dual-purpose nonoverlapping coil sets for both MOD and DoP, which are located on the power supply coil, are newly proposed. The proposed nonoverlapping coil sets can be easily fabricated using a flexible PCB. The existence of metal objects on the power supply coil is determined by the induced voltage difference of the nonoverlapping coil sets, and the position of the EV is simultaneously determined by induced voltage of the nonoverlapping coil sets. The proposed MOD and DoP methods do not contribute to any power loss, and thus, the efficiency of the IPTS for wireless stationary EV chargers can be maintained without additional power losses. The proposed nonoverlapping coil sets have been demonstrated by simulations and experiments with a prototype of the nonoverlapping coil sets and a developed sensing circuit.

II. Nonoverlapping Coil Sets for MOD and DoP

A. Overall Configuration of the Proposed Coil Sets

In general, the IPTS for wireless stationary EV chargers consist of two subsystems:

1) a transmitter subsystem to provide power, consisting of a utility frequency rectifier, a high-frequency inverter, a primary capacitor bank, and a power supply coil including cores and power cables; and
2) an on-board subsystem to receive the required power from the transmitter subsystem. It includes the pick-up coil including cores and power cables, a secondary capacitor bank, a high-frequency rectifier, and a dc–dc regulator.

The nonoverlapping coil system for MOD and DoP, composed of many pairs of the proposed coil set, are installed on the power supply coil. As shown in Fig. 1, the proposed coil sets are categorized into two coil sets based on their role: one is lateral coil sets to obtain the lateral location information of metal objects and EVs on the power supply coil and the other is for the longitudinal location information. In practice, lateral and longitudinal coil sets can overlap each other and they are located on the power supply coil to simultaneously obtain both lateral and longitudinal information for MOD and DoP. In Fig. 1, these two different coil sets are spatially separated for a better understanding of the readers.

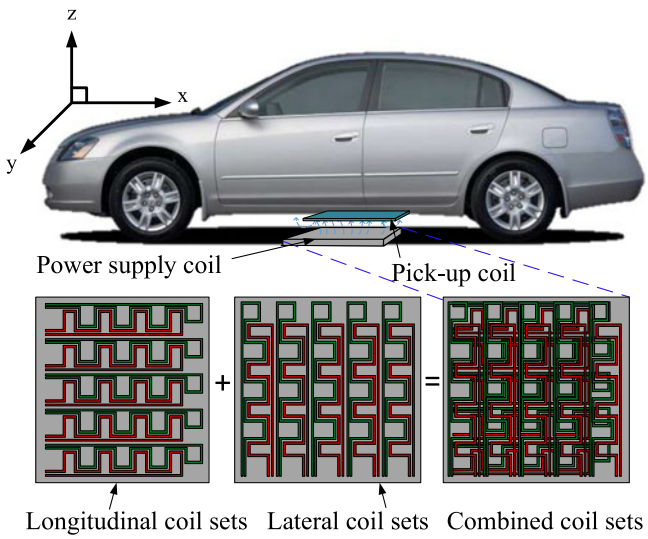

Fig. 1. Configuration of a wireless stationary EV charger with the proposed nonoverlapping coil sets.

When AC magnetic field is applied to metallic objects, eddy current is generated in the metallic objects [26]. The eddy current increases ohmic power loss of metallic objects, which may result in high temperature for the case of large resistance in the metallic objects. The skin depth of metallic objects δ for ac magnetic field is given as follows:

$$\delta = \sqrt{\frac{2}{\mu\omega\sigma}} \tag{1}$$

where δ is a function of permeability, angular frequency, and conductivity. The value of δ for an aluminum sheet at 85 kHz is 0.28 mm [26], which is typically much larger than the thickness of the aluminum sheet. For a thin aluminum sheet less than the skin depth, the thinner the hotter, because of larger resistance due to reduced effective conduction area.

B. Proposed Nonoverlapping Coil Sets for MOD

As shown in Fig. 2(a), the proposed nonoverlapping sets consist of two nonoverlapping symmetric coils, D- and Q-coils.

When the power supply coil is engaged by high-frequency current, the induced voltages of the D- and Q-coils can be calculated from Faraday's law as follows:

$$v_d = -\frac{d\,\phi_d}{dt} \tag{2a}$$

$$v_q = -\frac{d\,\phi_q}{dt} \tag{2b}$$

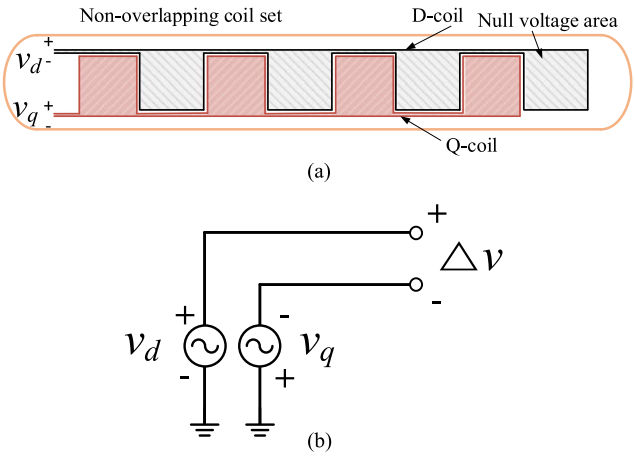

Fig. 2. Nonoverlapping coil set. (a) Configuration. (b) Principle to obtain the induced voltage difference.

where the time-varying induced voltages of the D- and Q- coils are v_d and v_q, respectively. ϕ_q and ϕ_d denote the magnetic fluxes generated by the power supply coil to pass through cross-section of the D- and Q-coils, respectively. The induced voltage difference is defined as follows:

$$\Delta v = v_d - v_q. \tag{3}$$

Their magnetic poles are symmetrically arranged to obtain the same induced voltages when the power supply coil generates magnetic fluxes during EV charging. A reference voltage, which is ideally zero from (3), can then be obtained by connecting D- and Q-coils in reverse direction to each other when there are no metal objects on the power supply coil, as shown in Fig. 2(b). If there are metal objects on the power supply coil, magnetic fluxes are distorted by eddy current induced in metal objects, and thereby the induced voltage difference is no longer zero. The MOD system can then detect the presence of metal objects by using the variation of the induced voltage difference. The nonoverlapping coil has a very small width to avoid deterioration in power transfer efficiency due to proximity effect. Furthermore, the coil is connected to so high impedance sensing circuit that no large circulating eddy current may flow.

In practice, the magnetic fluxes generated by the power supply coil are not uniform through the D- and Q-coils. Therefore, the null voltage area, which can be manually increased or decreased at the design level, should be considered with the understanding of the distribution of the magnetic fluxes on the power supply coil so that the reference voltage can be zero or nearly zero. In order to determine the feasibility of the proposed nonoverlapping sets for MOD, a model using finite element method simulations by ANSYS MAXWELL 15 has been designed, as shown in Fig. 3. In the simulation, only a single nonoverlapping coil set was used to assess its feasibility and the dimensions of the power supply coil as well as those of the nonoverlapping coil set are listed in Table I.

To verify the proposed concept, copper coins are employed as metal objects where coins were placed inside the D-coil. As shown in Fig. 4, the induced voltage difference between the D- and Q-coils increases as the number of coin increases.

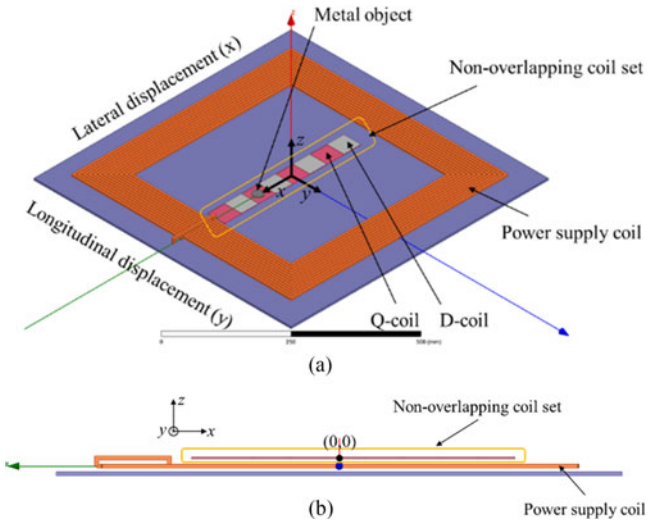

Fig. 3. FEA simulation model of the proposed nonoverlapping coil set for MOD with the power supply coil. (a) Bird's view. (b) Front view.

TABLE I
SIMULATION PARAMETERS OF NONOVERLAPPING COIL SET

Parameter	Value
Ferrite core of the power supply coil	$600 \times 440 \times 8$ mm^3
Outer dimension of the power supply coil	540×380 mm^2
Inner dimension of the power supply coil	410×250 mm^2
Size of nonoverlapping coil set	360×45 mm^2
The number of turns	20
Current of the power supply coil	20 A
Size of coin	4.5 cm^2

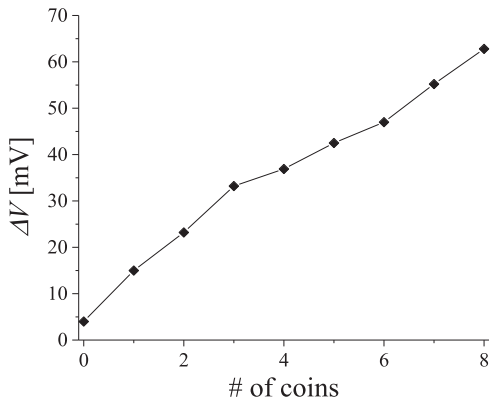

Fig. 4. Simulation results of the induced voltage difference of the nonoverlapping coil set along to the number of coins.

The reference voltage is initially adjusted to 4.16 mV and the induced voltage difference increases up to 62.8 mV with eight coins on the power supply coil.

C. Proposed Nonoverlapping Coil Sets for DoP

DoP of an EV to align the power supply coil and the pick-up coil for efficient power transfer is also an important issue. Moreover, for the voltage source series–series compensation

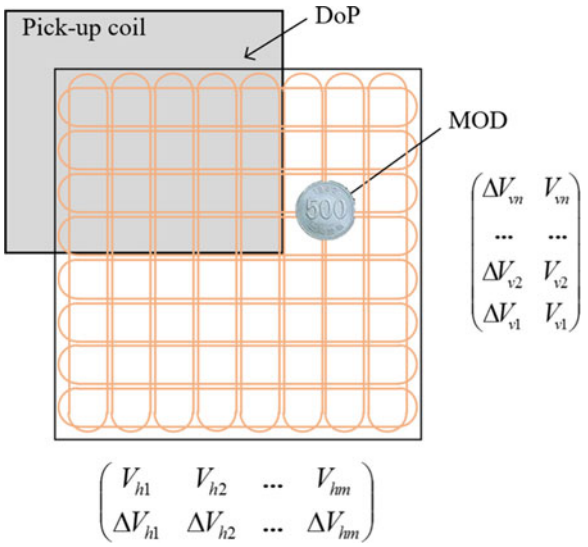

Fig. 5. Simplified configuration for the proposed nonoverlapping coil sets for both MOD and DoP.

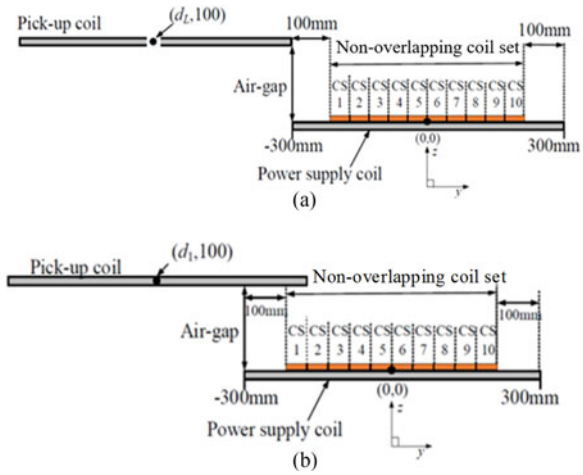

Fig. 6. Position of the pick-up with ten nonoverlapping coil sets for DoP. (a) Initial. (b) When the pick-up coil moves.

topology, the input and output currents increase with misalignment, resulting in an increase of the output power. As a result, a partial saturation in ferrite material can occur by increased current and fluxes deflected at one side. The induced voltage of each coil set has dependence on the pick-up coil since the distribution of magnetic fluxes on the power supply coil is changed by the ferrite material of the pick-up coil. Hence, the location of the pick-up coil for DoP can be found only by measuring the induced voltage of each coil set, as shown in Fig. 5, because magnetic fluxes passing through each coil set change and this leads to variation of the induced voltage of each coil set when the pick-up coil moves on the power supply coil.

The vehicle location is identified by measuring one of the induced voltages for the D- or Q-coils. The induced voltage can be calculated by using Faraday's law from (3). The threshold voltage of the D- or Q-coils, which determines whether the pick-up covers the coil sets, can be obtained by comparing the induced voltage variation as the pick-up moved over the power supply coil. In general, the induced voltage of the coil sets has its minimum value when the pick-up coil is far from the power supply coil while the induced voltage increases as the pick-up coil moves closer to the power supply coil. Therefore, the pick-up location can be identified by comparing the induced voltages among the matrix of the coil sets. When there are metal objects on the power supply coil, which also means they are on the nonoverlapping coil sets, the induced voltage difference of the nonoverlapping coil sets for MOD would have a nonzero value because the metal objects disturb magnetic fluxes passing through one of the D- and Q-coils. For example, metal objects on the power supply coil can be detected and their location also can be found by ΔV_{h6}, ΔV_{h7}, ΔV_{v5}, and ΔV_{v6}, as shown in Fig. 5.

In this paper, the feasibility of the proposed nonoverlapping coil sets for DoP has been studied by using an FEA simulation. In order to assess the feasibility of the proposed nonoverlapping coil sets for DoP, a simulation model has been designed, as shown in Fig. 6. In the simulation, ten nonoverlapping coil sets, i.e., CS1, CS2, ... and CS10, were used to determine the feasibility, and the parameters of the power supply coil and the nonoverlapping coil sets are listed in Table I.

At the initial condition, the center point of the pick-up coil along the y-axis is d_L of –600 mm, as shown in Fig. 6(a). As explained in the previous section, only the induced voltage v_q for the Q-coil is measured for DoP. When the pick-up coil moves closer to the power supply coil, v_d or v_q steadily increases based on the pick-up location. For example, if the center point of the pick-up coil is at the location $(-d_1, 100)$, as shown in Fig. 6(b), the pick-up coil fully covers the CS1. CS1, hence, will locally have a maximum induced voltage. By checking the induced voltage of the coil sets based on the reference value, the pick-up location can be identified.

As shown in Fig. 7, the simulation results for DoP show v_q for different air gaps and it is found that v_q of each Q-coil increases when the pick-up coil approaches each of them and reaches the peak value at the position where the pick-up coil fully covers a Q-coil. In this paper, only lateral misalignment and variation of air gap are considered to find the position of EV because angular misalignment and tilt between the power supply coil and pick-up coil are not significant in practice.

D. Sensing Circuit for MOD and DoP

The induced voltage difference can be matched at zero by adjusting the null voltage area, similar to the conventional overlapping coil. However, it is not easy to make all coil sets to zero in practice due to the uneven magnetic flux on the power supply coil. Even if it is possible to make induced voltage difference of all coil sets to zero, the induced voltage difference will no longer be guaranteed as zero when misalignment of an EV occurs accompanying the phenomenon that magnetic flux is deflected to one side.

The sensing signals should be converted to a dc value because sensing the time-varying signals, which have high frequency and many channels, not only requires high clock speed to the microcontroller but also many analog–digital converter (ADC)

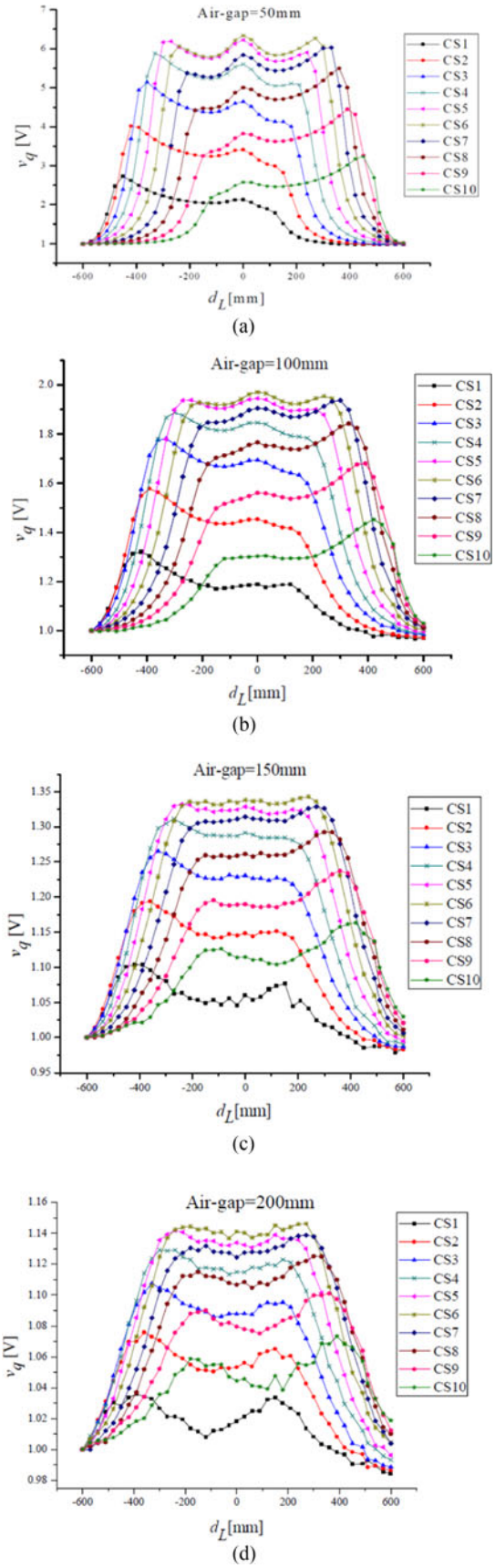

Fig. 7. Simulation results of the DoP for the Q-coils with the different air gaps such as (a) 50 mm, (b) 100 mm, (c) 150 mm, and (d) 200 mm.

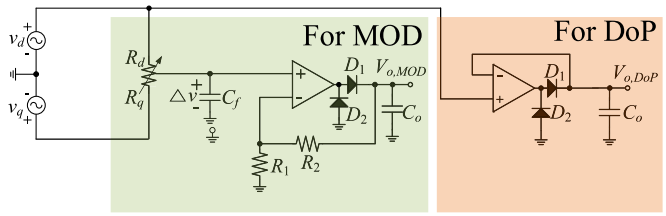

Fig. 8. Proposed sensing circuit for MOD based on a three-node sensing variable resistor.

channels. In case the induced voltage difference is not zero, which means that magnetic flux is larger at one side, the metal objects may not be detected even if they are placed on the power supply coil. The most important factor for MOD is the relative variation of the induced voltage difference value compared to the case without metal objects. For example, when metal objects are placed on the D-coil, which has larger induced voltage than the Q-coil, the induced voltage of the D-coil decreases. The metal objects may not be detected when the amount of voltage reduction of the D-coil is twice that of the reference value; only the phase of the induced voltage difference is reversed and the magnitude of the voltage difference does not change. This phenomenon can be accompanied by a more serious problem if the reference voltage is higher. As a remedy for this problem of the overlapping coil, a sensing circuit with a variable resistor to control the induced voltage at a minimum value, as shown in Fig. 8, was proposed.

Calibration and precise measurements are required as mandatory for mass production and repeatable systems. Although calibration is performed in factory considering magnetic field distribution of the power supply coil set, the voltage difference in each coil set cannot be zero due to the distortion of magnetic field by misalignments in practice. It is impossible to adjust the resistance value by human hands each time before starting wireless charging to keep the voltage differences as minimum values. To solve this problem, a digital potentiometer, whose resistance value is digitally controlled by a microcontroller unit for calibration, is adopted in this paper.

The induced voltage difference by a variable resistor without connecting any circuit is defined as follows:

$$\Delta v = \frac{v_d R_q - v_q R_d}{R_d + R_q}. \tag{4}$$

The impedance does not affect the induced voltage difference in the conventional sensing methods based on two-node measurement, whereas the proposed three-node sensing circuit based on a variable resistor can control the induced voltage difference. This method not only makes the induced voltage difference zero but also provides position monitoring for DoP. As mentioned in the previous section, although the nonoverlapping coil sets are inductively coupled with a power supply coil, the influence is not significant if the resistance of the sensing circuit is very large. The variable resistor should be designed to have a higher resistance than the internal resistor of the coil sets for two main reasons: the first is to reduce the influence of reactance of the coil sets to make the difference in the induced voltage zero

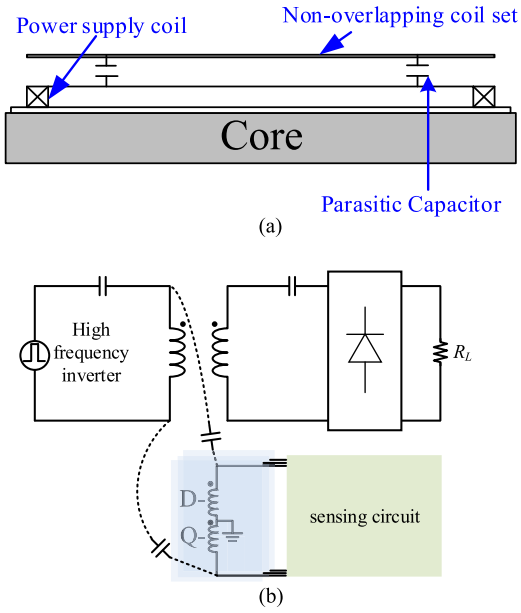

Fig. 9. Parasitic coupling effect of the nonoverlapping coil sets by capacitive coupling. (a) Side-view of the power supply coil and nonoverlapping coil sets. (b) Its equivalent circuit.

and the second is to reduce the circulating current of the sensing coil. In many cases, the difference in the induced voltage of each coil reaches several hundreds of millivolts with a few ohms of internal resistance. If a variable resistor with a lower value of resistance is connected to the nonoverlapping coil sets in series, the nominal allowable current density of the nonoverlapping coil will be exceeded, resulting in damage to the nonoverlapping coil sets.

The sensing circuit is vulnerable to noise because Δv of the circuit for MOD basically is close to zero. According to SAE J2954, the nominal switching frequency is assigned as 85 kHz. The inverter generates 85 kHz square voltage using semiconductor switches. High-frequency harmonics by gate drivers or power semiconductor switches will be injected to the power supply coil, and the high-frequency harmonics eventually will be coupled to the nonoverlapping coil sets, which is placed close to the power supply coil, through parasitic capacitive coupling, as shown in Fig. 9. Therefore, switching noise attenuation is necessary, and a simple method to reduce the noise is introduced in this section.

The largest portion of the noise is harmonics generated by a high-frequency inverter through capacitive coupling between power supply coil and nonoverlapping coil sets. The harmonic noise deteriorates the level of confidence in detection, which needs to be statistically described, though not shown in this paper. One way to reduce the harmonic noise is to apply a sinusoidal voltage source instead of a square wave to the power supply coil using *LCC* compensation or dummy inductors in series with the power supply coil. To reduce the harmonic noise without any modification of the power supply coil, a passive first-order *RC* low-pass filter (LPF), which contains R_d, R_q, and C_f, is added to the sensing circuit, as shown in Fig. 8. The transfer function $H(j\omega)$ is defined as follows:

$$H_d\left(j\omega\right) = \frac{1}{1+j\omega C_f R_d} \tag{5a}$$

$$H_q\left(j\omega\right) = \frac{1}{1+j\omega C_f R_q}. \tag{5b}$$

A first-order *RC* LPF, which has an identical cut-off frequency to the fundamental frequency, is designed because the majority of harmonics are high frequency having a band of several megahertz. Hence, zero voltage adjustment and noise filtering are achieved simultaneously with C_f. The induced voltage is derived as follows:

$$\Delta V = H_d\left(j\omega\right)\cdot V_d - H_q\left(j\omega\right)\cdot V_q. \tag{6}$$

Although most noise is rejected by the *RC* LPF, ΔV still has a small value. If the size of the metal is too small, it is difficult to distinguish between noise and a small voltage difference. Thus, the differential voltage of the MOD circuit should be amplified. R_1, R_2, and op-amp incorporate a noninverting precision amplifier, and its output voltage $V_{o,MOD}$ is determined as follows:

$$V_{o,MOD} = \sqrt{2}\left(1+\frac{R_1}{R_1}\right)\Delta V. \tag{7}$$

The output voltage $V_{o,MOD}$ should be a dc value considering system performance and cost. If the output voltage is an ac signal, a high-performance ADC is needed to obtain the exact signal, and it is very sensitive to noise. Diode D_1 and the op-amp play a role of a positive half-wave precision rectifier to remove the forward voltage drop by the diode because $V_{o,MOD}$ is much smaller than the voltage drop of the diode, and the MOD circuit cannot detect a small metal object without precision rectification. The capacitor C_0 makes the dc voltage equal to the peak value of the ac signal. D_2 is placed parallel to the output of the op-amp to avoid negative saturation, resulting in a decrease of the maximum slew rate of the op-amp. Thus, it enhances the accuracy of the signal processing. Finally, the ADC reads the dc voltage and information is sent to the high-frequency inverter through wired or wireless communication. In the case of the circuit for DoP, a half-wave precision rectifier, which has high input impedance, is also adopted because the induced voltage v_d or v_q is large enough and the DoP sensing circuit must be separate from the MOD sensing circuit. The rest of the circuit operating is omitted because the other parts are the same as the sensing circuit for MOD, and the output voltage of the sensing circuit for DoP $V_{o,MOD}$ is determined as follows:

$$V_{o,\mathrm{PoD}} = \sqrt{2}V_d. \tag{8}$$

E. Dead Zone of MOD and Diagram of Operating Sequence

However, the voltage difference could still be zero even when metal objects are situated on the power supply coil and they cover the same area on both the D- and Q-coils, as shown in Fig. 10(a). As a solution to this problem, additional coil sets, which are exactly the same as the D and Q-coils, are diagonally located to the previous coil sets to cover the dead zone problem of the proposed coil sets, as shown in Fig. 10(b).

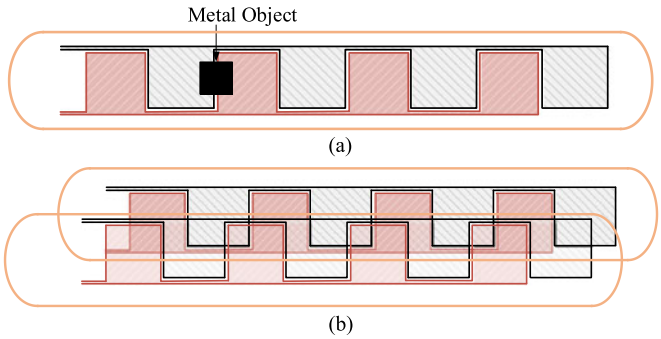

Fig. 10. Proposed nonoverlapping coil sets. (a) Example of a dead zone. (b) A method for dead zone avoidance.

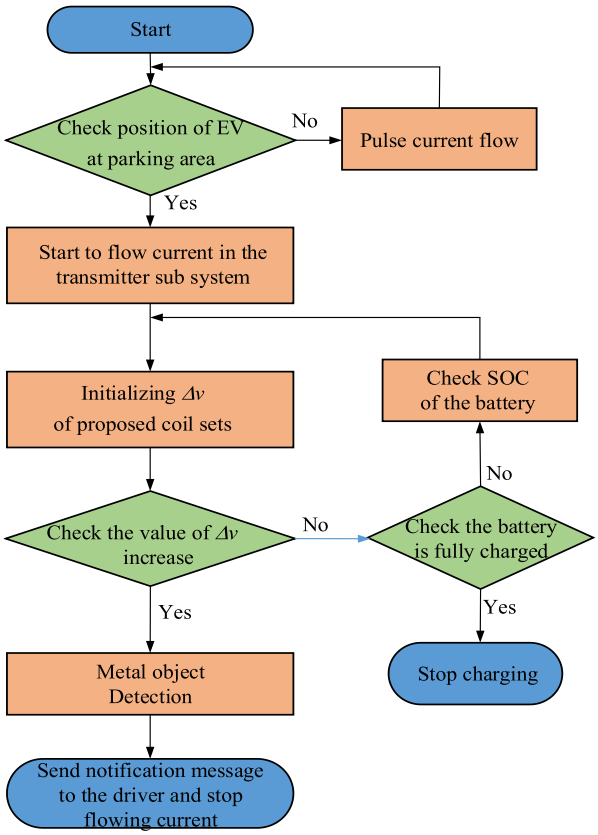

Fig. 11. Operating diagram of nonoverlapping coil sets for MOD.

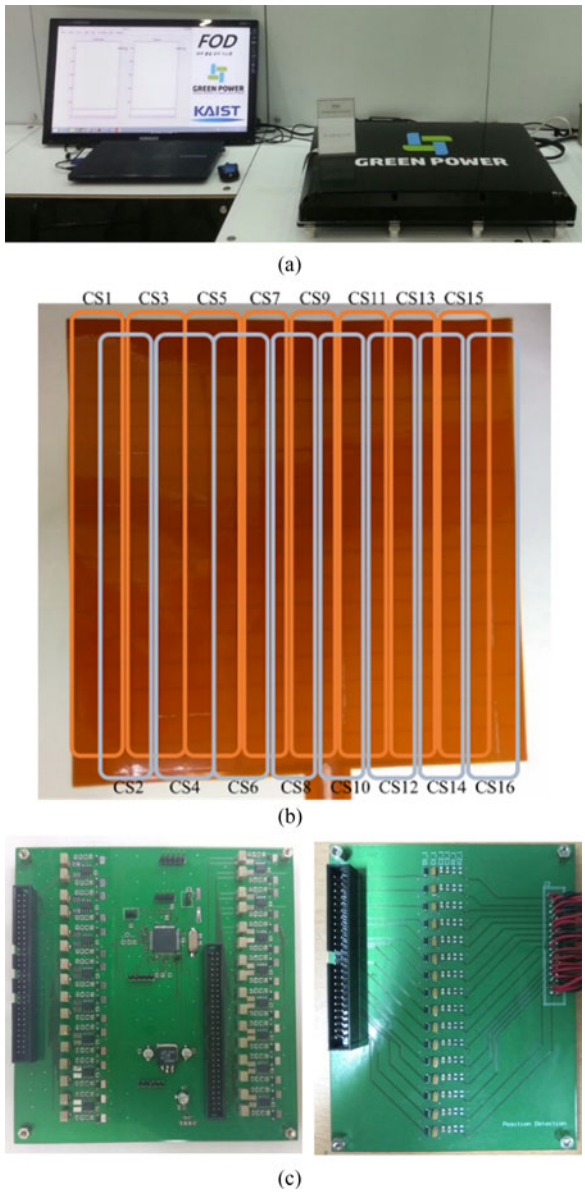

Fig. 12. Experimental setup of the proposed nonoverlapping coil sets with the power supply coil. (a) Overall configuration. (b) Nonoverlapping coil sets. (c) Sensing circuit for MOD and DoP.

The operating diagram of the nonoverlapping coil sets for MOD is explained by a flowchart in Fig. 11. For example, first, check the parking area is checked for the presence of a vehicle. If there is no vehicle on the power supply coil, then the power supply coil is turned OFF. On the other hand, it starts to flow some current into the power supply coil to check for metal objects. The voltage differences of the coil sets are then measured and any nonzero values among the coil sets are detected. If a voltage difference is higher than the threshold value, which can be determined by trial and error, then the current supply to the power supply coil is stopped and a notification message to the driver to remove the objects on the power supply coil is sent. On the other hand, if all the voltage differences are zero, the charging state of a battery is checked with respect to whether it is 100%. If not, current is flowed into the power supply coil to charge the vehicle. Finally, when the battery is fully charged, the EV charging process is stopped.

III. Experimental Verifications

In order to verify the feasibility of the proposed nonoverlapping coil sets, an experimental setup has been fabricated on the power supply coil, as shown in Fig. 12. The proposed MOD system was integrated into the power supply coil. Here, the system operating frequency is chosen as 85 kHz, which is in the standard range determined by the SAE J2954 drafted by the SAE task force, where the nominal frequency range is from 81.38 to 90.00 kHz for a light-duty passenger EV. The resonance topology adopts series–series compensation with phase shift control

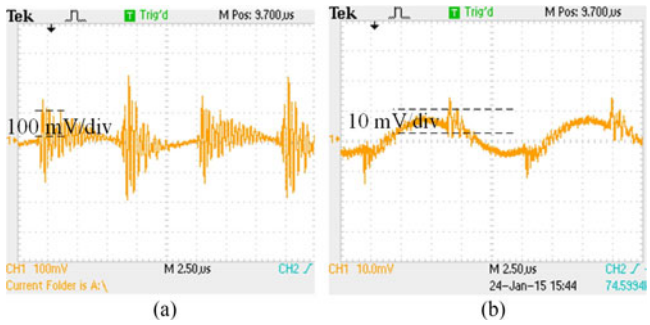

Fig. 13. Voltage difference including high-frequency noise. (a) Without and (b) with the filter.

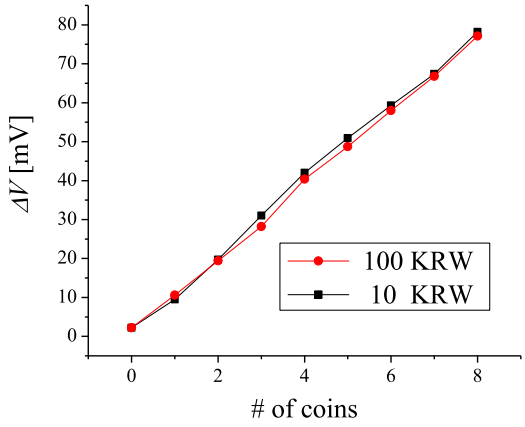

Fig. 14. Measured voltage difference according to the number of coins.

to regulate the current. To mimic the film coil structure, which will be used for commercialization, a flexible PCB, which has a very thin dielectric copper, with a thickness of 0.05 mm and a width of 0.1 mm, has been selected to fabricate the nonoverlapping coil sets, while an acetal cover with 7 mm thickness has been placed between the nonoverlapping coil sets and the power supply coil. The nonoverlapping coil system is located at the center of the power supply coil because of its symmetric configuration. In this paper, the size of the nonoverlapping coil system was made to be a little smaller than that of the power supply coil due to fabrication limit. On the other hand, the size of a nonoverlapping coil set is related to the size of metallic objects, for example, a small size of the coil sets if required for the detection of a small metallic object. The sensing circuit with an aluminum shielding plate was integrated into the bottom of the ferrite core to reduce the effect of the leakage flux. The other dimensions and circuit parameters of the fabricated prototype are appropriately designed to correspond with the simulation.

A. Experimental Verification for MOD

It is found that there will be a large amount of noise in the induced voltages of the coil sets produced by high-frequency ringing due to parasitic capacitances between the coil sets and the power supply coil. As shown in Fig. 9(b), most high-order harmonics will be applied to the power supply coil, which has relatively high impedance, instead of a compensation capacitor when square voltage is applied. The high-frequency noise passes into the sensing circuit through the parasitic capacitive coupling between the coil sets and the power supply coil. Therefore, it is difficult to set the reference voltage difference as a zero value without a filter. In order to reduce the noise, a simple low-pass *RC* filter with a cut-off frequency of 81 kHz, which is slightly lower than the operating frequency, is chosen to effectively reduce high-frequency components. The resistance $R_d + R_q$ and capacitance C_f have been selected as 10 kΩ and 0.2 nF by using the cut-off frequency. Although the amplitude of the fundamental frequency is reduced by around –3 dB, the ratio of noise reduction may be designed to be much larger.

As shown in Fig. 13, the high-frequency noise was significantly reduced by 10 mV by the LPF. Actually, the induced voltage difference cannot be completely symmetrical, and there are some factors responsible for this such as temperature drift, external vibration, unintentional loop area of the oscilloscope probe, and mismatch of the reactance of the nonoverlapping coil sets. All of the aforementioned may lead to fluctuation in the sensing circuit, which has a strong influence on metal detection. In order to eliminate the fluctuation effect, data were continuously collected for five voltage signals in the experiment and the average value was calculated.

The results were collected by serial communication between the MOD system and a laptop using MATLAB. Optical communication is used for stable data transfer since data loss should occur by the magnetic coupling noise to the communication channel. In order to verify the proposed nonoverlapping coil sets for MOD, the reference voltage is set to be less than 10 mV by changing the variable resistor value of the sensing circuit without any metal object. Two different coins, 10 and 100 Korean Won (KRW), which are, respectively, composed of iron and copper, were used as metal objects. As shown in Fig. 14, the experimental results show a good agreement with the simulation results for MOD because the voltage difference linearly increases with respect to the number of coins on the power supply coil. However, there is no substantial voltage difference between the two different coins even though their areas are different. This is because there is only a small area difference between them, 4.5 cm^2 for 100 KRW and 4.1 cm^2 for 10 KRW.

Fig. 15 shows experimental results with vertical and horizontal nonoverlapping coil sets for recognition and position of multiple metal objects. The threshold voltage was arbitrarily set as 50 mV for stable operation. The MOD system can detect not only the presence but also the coordinates of an aluminum sheet with different positions, as shown in Fig. 15(a) and (b). Specifically, a 3×2 cm^2 aluminum sheet is placed on the nonoverlapping coil sets with coordinates of 5 horizontal and 9 vertical, and 12 horizontal and 9 vertical, respectively. To verify detection of multiple metal objects, an additional aluminum sheet, which is 2×2 cm^2 in size, is used for the experiments, as shown in Fig. 15(d). An additional red bar graph appeared when a 2×2 cm^2 aluminum sheet is additionally placed on the nonoverlapping coil sets at coordinates of 2 horizontal and 8 vertical. Although a voltage variation of the 2×2 cm^2 aluminum

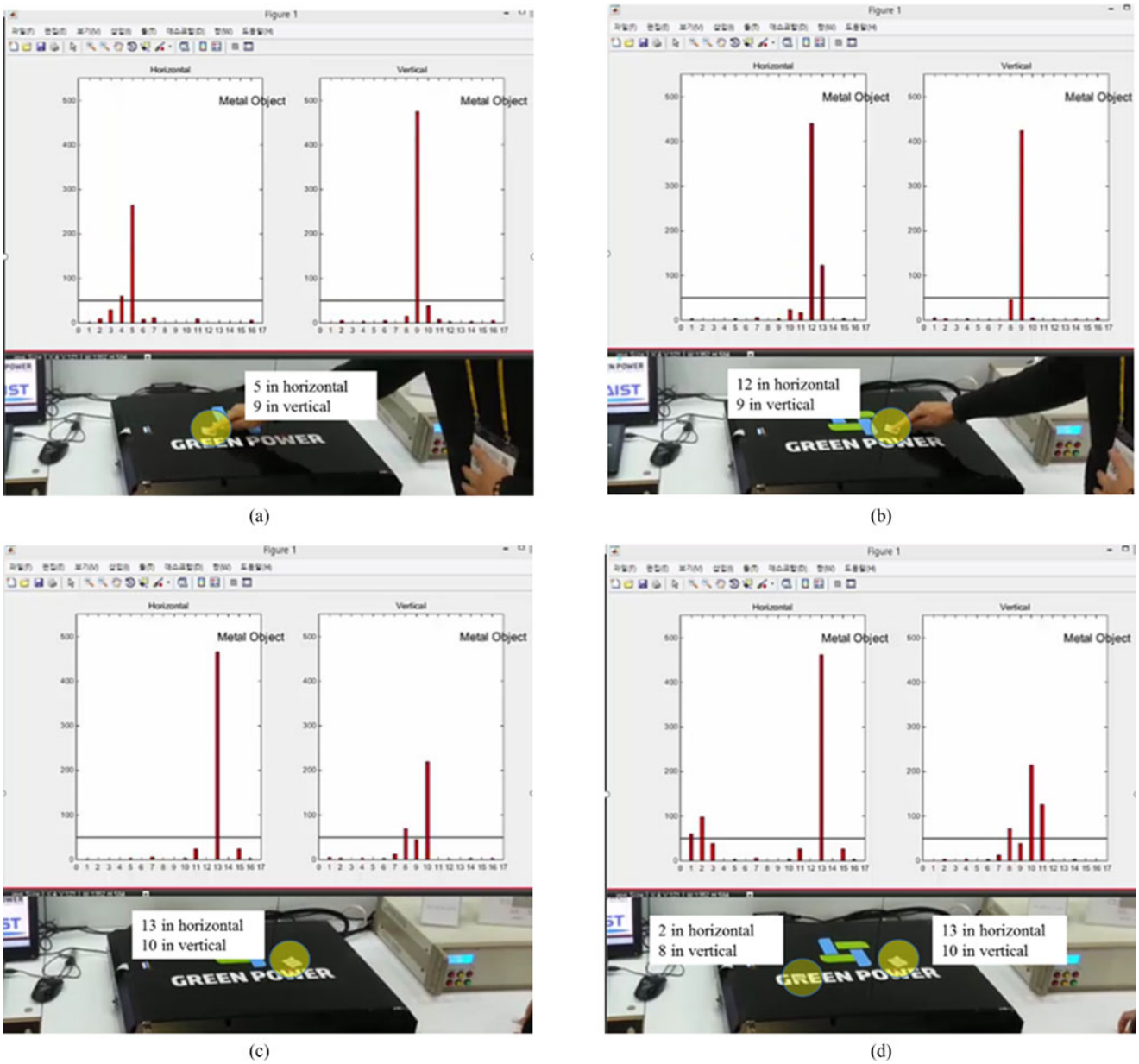

Fig. 15. Measurement monitoring system depending on the positions of the metal objects. (a) With 2 × 3 cm^2 aluminum sheet at 5 horizontal and 9 vertical. (b) With 2 × 3 cm^2 aluminum sheet at 12 horizontal and 9 vertical. (c) With 2 × 3 cm^2 aluminum sheet at 13 horizontal and 10 vertical. (d) With (c) and 2 × 2 cm^2 aluminum sheet at 2 horizontal and 8 vertical.

sheet is eight times smaller than that of the larger aluminum sheet, it can still detect the aluminum sheet.

B. Experimental Verification for DoP

To verify the feasibility of DoP, a ferrite core having a size of 600 × 400 mm^2 was used for the pick-up coil, as shown in Fig. 16. Where the air gap is 10 cm, the dimension of the nonoverlapping coil sets is the same as the simulation conditions mentioned in the previous section. The data were collected by LABVIEW since a vast amount of data must be stored and postprocessed according to the position of the pick-up coil.

The data for all nonoverlapping coil sets were collected and only the results for seven nonoverlapping coil sets are shown in Fig. 17, due to the better understanding of readers and the complexity of data expression. The ninth nonoverlapping coil set is symmetrically centered with respect to the power supply coil. $V_{o,DoP}$ is normalized based on when the pick-up coil is far from the power supply coil. The normalized $V_{o,DoP}$ increased roughly 1.6 times compared to without the ferrite core of the pick-up coil.

This shows that as the pick-up coil approaches the power supply coil, the magnetic reluctance on the power supply coil near the pick-up coil is reduced by the ferrite core of the pick-up coil, resulting in an increase of $V_{o,DoP}$. The point where the maximum voltage occurs depends on the coil sets design; however, if the expected results are obtained through the simulation, the

(a)

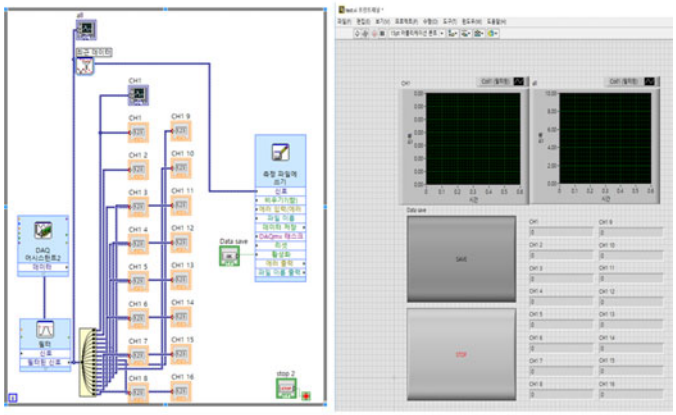

(b)

Fig. 16. (a) Experimental setup of proposed nonoverlapping coil sets for DoP and (b) the measurement monitoring system.

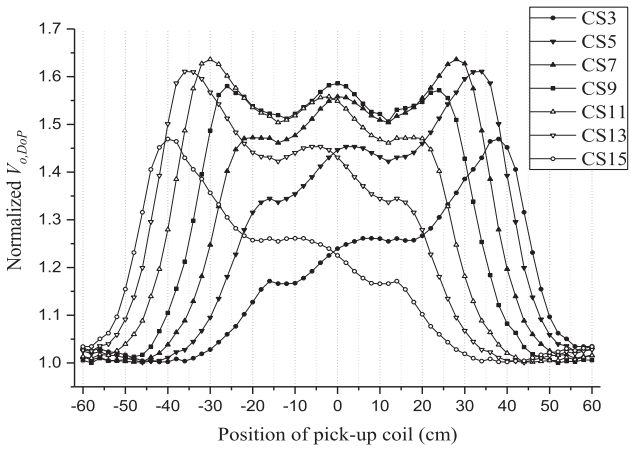

Fig. 17. Measured normalized $V_{o,DoP}$ with respect to the position of the pick-up coil.

position can be inferred. Although there is a slight discrepancy between the simulation results and experimental results, the tendencies of the normalized $V_{o,DoP}$ of each nonoverlapping coil set are well matched with the simulation results of Fig. 7.

IV. Conclusion

In this paper, novel dual-purpose nonoverlapping coil sets, which detect a variation of magnetic flux on the power supply coil, for both MOD and DoP have been newly introduced, and it was verified that the proposed MOD and DoP methods do not contribute to any power losses. With the induced voltage difference of the nonoverlapping coil sets, the existence of metal objects as well as their location can be found for MOD. When metallic coins and aluminum sheets are located on the power supply coil, the induced voltage difference of the coil sets, which is ideally zero without metal objects, significantly increases to 62.8 and 450 mV, respectively, which is more than ten times the value without metal objects throughout the experiments. At the same time, the position of the pick-up coil can be identified for DoP by the induced voltage variation of the coil sets when the pick-up coil arrives on the power supply coil. It is demonstrated in this work that both MOD and DoP can be achieved by the proposed nonoverlapping coil sets without any power losses.

References

[1] S. Y. Choi, S. Y. Jeong, E. S. Lee, B. W. Gu, S. W. Lee, and C. T. Rim, "Generalized models on self-decoupled dual pick-up coils for a large lateral tolerance," *IEEE Trans. Power Electron.*, vol. 30, no. 11, pp. 6434–6445, Nov. 2015.

[2] S. Y. Choi, B. W. Gu, S. Y. Jeong, and C. T. Rim, "Trends of wireless power transfer systems for roadway powered electric vehicles," in *Proc. IEEE VTC Workshop Emerging Technol., Wireless Power*, May 2014, pp. 31–35.

[3] S. Y. Choi, B. W. Gu, S. Y. Jeong, and C. T. Rim, "Ultra-slim S-type inductive power transfer system for roadway powered electric vehicles," in *Proc. Int. Electr. Vehicle Technol. Conf. Automot. Power Electron. Japan*, May 2014, pp. 1–7.

[4] A. Shafiei and S. S. Williamson, "Plug-in hybrid electric vehicle charging: Current issues and future challenges," in *Proc. IEEE Vehicle Power Propulsion Conf.*, 2010, pp. 1–8.

[5] C. Y. Huang, J. T. Boys, G. A. Covic, and M. Budhia, "Practical considerations for designing IPT system for EV battery charging," in *Proc. IEEE Vehicle Power Propulsion Conf.*, 2009, pp. 402–407.

[6] H. H. Wu, A. Gilchrist, K. Sealy, P. Israelsen, and J. Muhs, "A review on inductive charging for electric vehicles," in *Proc. IEEE Int. Electr. Mach. Drives Conf.*, 2011, pp. 143–147.

[7] K. Aditya and S. S. Williamson, "Design considerations for loosely coupled inductive power transfer (IPT) system for electric vehicle battery charging - A comprehensive review," in *Proc. IEEE Trans. Electrif. Conf. Expo*, 2014, pp. 1–6.

[8] S. Li and C. C. Mi, "Wireless power transfer for electric vehicle applications," *IEEE J. Emerging Sel. Topics Power Electron.*, vol. 3, no. 1, pp. 4–17, Mar. 2015.

[9] N. Kuyvenhoven, C. Dean, J. Melton, J. Schwannecke, and A. E. Umenei, "Development of a foreign object detection and analysis method for wireless power systems," in *Proc. IEEE Symp. Product Compliance Eng.*, 2011, pp. 1–6.

[10] S. Fukuda, H. Nakano, Y. Murayama, T. Murakami, O. Kozakai, and K. Fujimaki, "A novel metal detector using the quality factor of the secondary coil for wireless power transfer systems," in *Proc. IEEE Int. Microw. Workshop Ser. Innov. Wireless Power Transm., Technol. Syst. Appl.*, 2012, pp. 241–244.

[11] S. Verghese, M. P. Kesler, K. L. Hall, and H. T. Lou, "Foreign object detection in wireless energy transfer systems," Patent US 20 130 069 441 A1, Sep. 9, 2011.

[12] M. R. Sonapreetha, S. Y. Jeong, S. Y. Choi, and C. T. Rim, "Dual-purpose non-overlapped coil sets as foreign object and vehicle location detections for wireless stationary EV chargers," in *Proc. 2015 IEEE PELS Workshop Emerging Technol. Wireless Power*, 2015, pp. 1–7.
[13] "SAE J2954 overview and path forward." [Online]. Available: http://www.sae.org/smartgrid/sae-j2954-status_1-2012.PoDf
[14] X. Qunyu, N. Huansheng, and C. Weishi, "Video-based foreign object debris detection," in *Proc. IEEE Int. Workshop Imag. Syst. Techn.*, 2009, pp. 119–122.
[15] S. Futatsumori, K. Morioka, A. Kohmura, and N. Yonemoto, "Design and measurement of W-band offset stepped parabolic reflector antennas for airport surface foreign object debris detection radar systems," in *Proc. IEEE Int. Workshop Antenna Technol.*, 2014, pp. 51–52.
[16] T. Kato, Y. Ninomiya, and I. Masaki, "An obstacle detection method by fusion of radar and motion stereo," *IEEE Trans. Intell. Transp. Syst.*, vol. 3, no. 3, pp. 182–188, Sep. 2002.
[17] A. Kohmura, S. Futatsumori, N. Yonemoto, and K. Okada, "Fiber connected millimeter-wave radar for FOD detection on runway," in *Proc. IEEE Eur. Radar Conf.*, 2013, pp. 41–44.
[18] Z. N. Low, J. J. Casanova, P. H. Maier, J. A. Taylor, R. A. Chinga, and J. Lin, "Method of load/fault detection for loosely coupled planar wireless power transfer system with power delivery tracking," *IEEE Trans. Ind. Electron.*, vol. 57, no. 10, pp. 1478–1486, Apr. 2010.
[19] G. Ombach, "Design considerations for wireless charging system for electric and plug-in hybrid vehicles," in *Proc. IEEE Hybrid Electr. Vehicles Conf.*, 2013, pp. 1–4.
[20] F. Dan, Z. Qi, and Y. Xuelian, "Electromagnetic characteristics simulation of airport runway FOD," in *Proc. IEEE Int. Workshop Microw. Millim. Wave Circuits Syst. Technol.*, 2013, pp. 13–16.
[21] H. Kikuchi, "Metal-loop effects in wireless power transfer systems analyzed by simulation and theory," in *Proc. IEEE Electr. Des. Adv. Packag. Syst. Symp.*, 2013, pp. 201–204.
[22] J. Svatos, J. Vedral, and P. Novacek, "Metal object detection and discrimination using Sinc signal," in *Proc. IEEE 13th Biennial Baltic Electron. Conf.*, 2012, pp. 307–310.
[23] L. S. Riggs and J. E. Mooney, "Identification of metallic mine-like objects using low frequency magnetic fields," *IEEE Trans. Geosci. Remote Sens.*, vol. 39, no. 1, pp. 56–66, Jan. 2001.
[24] D. C. Chin, R. Srinivasan, and R. E. Ball, "Discrimination of buried plastic and metal objects in subsurface soil," in *Proc. IEEE Geosci. Remote Sens. Symp.*, vol. 1, 1998, pp. 505–508.
[25] H. Kudo, K. Ogawa, N. Oodachi, and N. Deguchi, "Detection of a metal obstacle in wireless power transfer via magnetic resonance," in *Proc. IEEE 33rd Int. Telecommun. Energy Conf.*, 2011, pp. 1–6.
[26] B. Paul, J. Wright, and J. Z. Bird, "3-D steady-state eddy-current damping and stiffness terms for a finite thickness conductive plate," *IEEE Trans. Magn. Ind. Electron.*, vol. 50, no. 11, Nov. 2014, Art. no. 6301404.

Seog Y. Jeong (S'14) received the B.S. degree in electrical engineering from Kyungpook National University, Daegu, South Korea, in 2012, and the M.S. degree in nuclear quantum engineering in 2015 from Korea Advanced Institute of Science and Technology, Daejeon, South Korea, where he is currently working toward the Ph.D. degree.

His current research interests include roadway-powered electric vehicle and wireless power transfers.

Hyung G. Kwak (S'15) was born in South Korea, in 1990. He received the B.S. degree in electrical engineering from Inha University, Incheon, South Korea, in 2015, and the M.S degree in nuclear quantum engineering from Korea Advanced Institute of Science and Technology, Daejeon, South Korea, in 2017.

He has developed foreign object detection and wireless power transfer system. His current research interests include power converters and magnetics.

Gi C. Jang (S'15) received the B.S. degree in electrical and electronic engineering and the M.S. degree in nuclear and quantum engineering from Korea Advanced Institute of Science and Technology, Daejeon, South Korea, in 2012.

He is currently working as a Research Engineer with Hyundai KEFICO, Gunpo, South Korea. His research interests include the field of electronic control unit, and wireless power transfer system for hybrid and electric vehicles.

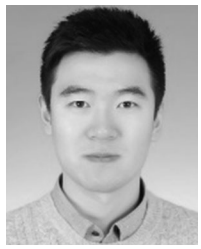

Su Y. Choi (S'13–M'16) received the B.S. degree in mechanical engineering from Pusan National University, Pusan, South Korea, in 2011, and Integrated Master's and Ph.D. degree in nuclear and quantum engineering from Korea Advanced Institute of Science and Technology, Daejeon, South Korea, in 2016.

Since 2017, he has been a Senior Researcher in the Hyper Tube eXpress Research Team, Korea Railroad Research Institute, Uiwang, South Korea. His current research interests include wireless power transfers, linear synchronous motors, and hyperloop.

Chun T. Rim (M'90–SM'11) received the B.S. degree (with Hons.) from Kumoh Institute of Technology, Gumi, South Korea, in 1985, and the M.S. and Ph.D. degrees from Korea Advanced Institute of Science and Technology (KAIST), Daejeon, South Korea, in 1987 and 1990, respectively, all in electrical engineering.

From 2007 to 2016, he was an Associate Professor with KAIST. Currently, he is a Full Professor with the Gwangju Institute of Science and Technology, Gwangju, South Korea. He has authored or coauthored 160 technical papers, written 14 books, and holds 150 patents (awarded and pending).

Dr. Rim has received numerous awards, including the Best Paper Award of the IEEE TRANSACTIONS ON POWER ELECTRONICS (IEEE TPEL) in 2015 and the IEEE JOURNAL OF EMERGING AND SELECTED TOPIC IN POWER ELECTRONICS (IEEE J-ESTPE) in 2016, both in wireless power transfer (WPT). He is currently an Associate Editor for the IEEE TPEL and the IEEE J-ESTPE, a Guest Editor of the Special Issue on WPT of the IEEE TPEL, the IEEE TRANSACTIONS ON INDUSTRIAL ELECTRONICS, and the IEEE J-ESTPE, and the General Chair of the 2015 and 2016 IEEE Workshop on Wireless Power.